Dispersion relation reconstruction for 2D Photonic Crystals based on polynomial interpolation

Yueqi Wang* and Guanglian Li†

Abstract

Dispersion relation reflects the dependence of wave frequency on its wave vector when the wave passes through certain materials. It demonstrates the properties of this material and thus it is critical. However, dispersion relation reconstruction is very time consuming and expensive. To address this bottleneck, we propose in this paper an efficient dispersion relation reconstruction scheme based on global polynomial interpolation for the approximation of 2-dimension photonic band functions. Our method relies on the fact that the band functions are piecewise analytic with respect to the wave vector in the first Brillouin zone. We utilize suitable sampling points in the first Brillouin zone at which we solve the eigenvalue problem involved in the band function calculation, and then employ Lagrange interpolation to approximate the band functions on the whole first Brillouin zone. Numerical results show that our proposed method can significantly improve the computational efficiency.

Key words: Photonic Crystals, band function, Lagrange Interpolation, sampling methods

1 Introduction

Photonic Crystals (PhCs) are periodic dielectric materials with size of their period comparable to the wavelength [17]. The propagation of electromagnetic waves inside such materials depends heavily on their frequencies. Furthermore, electromagnetic waves within a certain frequency range cannot propagate in certain PhCs. This forbidden frequency range is the so-called band gap, which motivates many important applications, including optical transistors, photonic fibers and low-loss optical mirrors [37, 27, 25, 35]. In this paper, we focus on 2-dimension PhCs which are periodic in the xy plane and homogeneous along the z axis with high-contrast dielectric columns or holes spaced in dielectric materials.

To fully understand PhCs, research interest falls on the propagating frequency as well as the band gap. The periodicity of PhCs allows using the Bloch's theorem so that the original Helmholtz eigenvalue problem on the whole space is transformed into a family of Helmholtz eigenvalue problems defined on the unit cell parameterized by the wave vector $\mathbf{k}$ varying in the irreducible Brillouin zone (IBZ) $\mathcal{B}_{\text{red}}$ [24]. The frequency ω_n which is a scaling of the square root of nth largest eigenvalue, regarded as a function of the wave vector $\mathbf{k}$ is the so-called the

*Department of Mathematics, The University of Hong Kong, Pokfulam Road, Hong Kong. Email: u3007895@connect.hku.hk

†Department of Mathematics, The University of Hong Kong, Pokfulam Road, Hong Kong. Email: lotusli@maths.hku.hk

nth band function for all $n \in \mathbb{N}^+$. The band gap is the distance between two adjacent band functions. Consequently, the calculation of the nth band function $\omega_n(\mathbf{k})$ involves solving infinite number of the Helmholtz eigenvalue problems defined on the unit cell parameterized by the wave vector $\mathbf{k} \in \mathcal{B}_{\text{red}}$, which have high-contrast and piecewise constant coefficients. To reduce this computational cost, a natural approach is to decrease the number of parameters $\mathbf{k}$ by limiting them to $\partial\mathcal{B}_{\text{red}}$. A practical approach is to discretize $\partial\mathcal{B}_{\text{red}}$ uniformly to generate the parameters. Although there is no rigorous theoretical foundation, this approach demonstrates its accuracy for many numerical tests on 2-dimension PhCs. To further reduce the number of parameters, several sampling algorithms have been proposed. In specific, Hussein introduced the model order reduction method to band gap calculation and proposed to use the high symmetry points and the intermediate points centrally intersecting the straight lines joining these high symmetry points as the sampling points [14]. Klindworth proposed to use Taylor expansion to approximate the reordered band functions based on the fact that band functions can be reordered so that they are analytic functions of $\mathbf{k}$ and an adaptive step size controlling was proposed to determine the sampling points [23]. In addition, some improvements to these methods have also been proposed in recent years [30, 18, 19].

1.1 Motivation for sampling inside $\mathcal{B}_{\text{red}}$

However, recently the question of whether $\partial\mathcal{B}_{\text{red}}$ are sufficient to characterize the band gap has received intensive interest. Figure 1 illustrates the extrema of the first six band functions of two 2-dimension PhCs as depicted in Figures 4 and 5. One can observe that they do not always appear over $\partial\mathcal{B}_{\text{red}}$. For example, Figure 1(d) depicts an extremum inside $\mathcal{B}_{\text{red}}$ which corresponds to the maximum value of the sixth band function. In Table 1 we present this maximum value and compare it with the maximum value of this case obtained using only $\partial\mathcal{B}_{\text{red}}$, which demonstrates the importance of the interior information. Furthermore, some work has shown counterexamples that highlight the dangers of just using $\partial\mathcal{B}_{\text{red}}$ [11, 26, 7]. Thus, it is urgent to develop an accurate and efficient sampling algorithm in the whole IBZ $\mathcal{B}_{\text{red}}$.

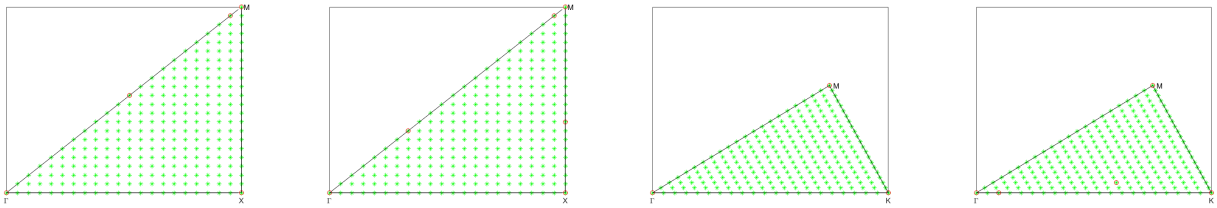

(a) Square lattice TM mode (b) Square lattice TE mode (c) Hexagonal lattice TM mode (d) Hexagonal lattice TE mode

Figure 1: Extrema exist at points marked with red circles, and green points are used to measure the extrema.

Nevertheless, to the best of our knowledge, there have been no trials in designing such kind of sampling algorithms. To fill this vacancy, we propose in this paper the use of several efficient sampling algorithms that can be combined with Lagrange interpolants to approximate band functions in $\mathcal{B}_{\text{red}}$. This work is built upon several well-developed sampling algorithms, which are wildly used in numerical approximation [1, 32, 3, 28, 6].

	$\mathcal{B}_{\text{red}}$		$\partial\mathcal{B}_{\text{red}}$	
Band number	$\mathbf{k}$	Extrema	$\mathbf{k}$	Extrema
6	$(0.719762, 0.049867)$	Maxi = 1.071796	$(0.690971, 0)$	Maxi = 1.069602

Table 1: Hexagonal lattice TE mode: band function's extrema obtained using $\mathcal{B}_{\text{red}}$and $\partial\mathcal{B}_{\text{red}}$.

1.2 Main contributions

Our main contributions are threefold. On the one hand, we analyze and summarize key regularity properties of band functions, cf. Theorems 3.2 and 3.6: First, band functions are piecewise analytic functions; Second, singularities occur only on branch points and the origin. These two results are proved by showing that $\{(\frac{\omega_n(\mathbf{k})}{c})^2\}_{n=1}^{\infty}$, which are referred to as the Bloch variety (3.1), are zeros of a real analytic function in $\mathbb{R}^3$. The locations of singular points are confirmed via implicit mapping theorem; Third, we give the formula for calculating the first partial derivatives of band functions at non-singularities, and thus point out that the first partial derivatives of band functions may be discontinuous at branch points where the dimension of the corresponding eigenspace is greater than one. This formula further reveals that band functions are Lipschitz continuous.

On the other hand, our proposed method can be utilized without resorting band functions which is crucial for the Taylor expansion based method as developed in [23]. Without resorting, we are allowed to approximate the first few band functions, which are the interest of many practical applications, while the aforementioned approach can only approximate the whole band functions simultaneously. Moreover, our method approximates band functions in the whole IBZ, and we can further incorporate it into many other numerical methods, e.g., adaptive FEM [9] and hp FEM [31], to calculate band functions with high accuracy and efficiency.

This paper is organized as follows. In Section 2, we describe the Maxwell eigenvalue problem involved in band structure calculation and elaborate on the derivation of the parameterized eigenvalue problem through Bloch's theorem as well as the two modes in two-dimension PhCs. Section 3 is concerned with the main regularity of the band functions, based upon which we introduce the numerical schemes to reconstruct these band functions in Section 4. Extensive numerical experiments are illustrated in Section 5 to support our theoretical findings. Finally, we present in Section 6 conclusions and future work.

2 Preliminaries

To study the propagation of light in Photonic Crystals, we begin with the macroscopic Maxwell equations. In SI convention, the Maxwell equations are composed of the following four equations [16]:

$$\begin{aligned} \nabla \times \boldsymbol{\mathcal{E}} + \frac{\partial \boldsymbol{\mathcal{B}}}{\partial t} &= 0, \\ \nabla \times \boldsymbol{\mathcal{H}} - \frac{\partial \boldsymbol{\mathcal{D}}}{\partial t} &= \boldsymbol{\mathcal{J}}, \\ \nabla \cdot \boldsymbol{\mathcal{D}} &= \rho, \\ \nabla \cdot \boldsymbol{\mathcal{B}} &= 0, \end{aligned}$$

where $\boldsymbol{\mathcal{E}}$ is the electric field, $\boldsymbol{\mathcal{H}}$ is the magnetic field, $\boldsymbol{\mathcal{D}}$ is the electric displacement field, $\boldsymbol{\mathcal{B}}$ is the magnetic induction field, $\boldsymbol{\mathcal{J}}$ is the free current density, ρ is the free charge density. Assuming there are no sources of light, we can set $\boldsymbol{\mathcal{J}} = \mathbf{0}$ and $\rho = 0$.

It is conventional to use the so-called constitutive relations to describe how $\boldsymbol{\mathcal{D}}$ and $\boldsymbol{\mathcal{B}}$ depend on $\boldsymbol{\mathcal{E}}$ and $\boldsymbol{\mathcal{H}}$. Strictly speaking, the constitutive relations are nonlinear. However, for most of the dielectric materials, we assume the field strengths are sufficiently weak and the materials are isotropic and nondispersive media, then it is reasonable to use the following linear approximations:

$$\begin{aligned}\boldsymbol{\mathcal{D}} &= \epsilon_0 \epsilon \boldsymbol{\mathcal{E}},\\ \boldsymbol{\mathcal{B}} &= \mu_0 \mu \boldsymbol{\mathcal{H}},\end{aligned}$$

where ϵ_0 is the vacuum permittivity, ϵ is the relative permittivity, μ_0 is the vacuum permeability, and μ is the relative magnetic permeability. Note that here both ϵ and μ are scalar functions that map points in $\mathbb{R}^3$ to $\mathbb{R}$ and $\epsilon, \mu \in L^\infty(\mathbb{R}^3)$. In most Photonic Crystals, it is assumed that the materials are nonmagnetic, i.e., $\mu \equiv 1$.

After introducing all of the above assumptions, the Maxwell equations can be formulated as

$$\nabla \times \boldsymbol{\mathcal{E}} + \mu_0 \frac{\partial \boldsymbol{\mathcal{H}}}{\partial t} = 0, \tag{2.1a}$$

$$\nabla \times \boldsymbol{\mathcal{H}} - \epsilon_0 \epsilon \frac{\partial \boldsymbol{\mathcal{E}}}{\partial t} = 0, \tag{2.1b}$$

$$\nabla \cdot (\epsilon \boldsymbol{\mathcal{E}}) = 0, \tag{2.1c}$$

$$\nabla \cdot \boldsymbol{\mathcal{H}} = 0. \tag{2.1d}$$

Here both $\boldsymbol{\mathcal{E}}$ and $\boldsymbol{\mathcal{H}}$ are functions of time and space, i.e., $\boldsymbol{\mathcal{E}} = \boldsymbol{\mathcal{E}}(\mathbf{x}, t)$, $\boldsymbol{\mathcal{H}} = \boldsymbol{\mathcal{H}}(\mathbf{x}, t)$, while the coefficients of these partial differential equations are time-independent. Thus, we can use the Fourier transformation in time domain to decompose the functions $\boldsymbol{\mathcal{E}}$ and $\boldsymbol{\mathcal{H}}$ depending on space and time into functions depending on spatial frequency, i.e.,

$$\begin{aligned}\mathbf{E}(\mathbf{x}) &:= (\mathcal{F}_t \boldsymbol{\mathcal{E}})(\mathbf{x}; \omega) = \int_{\mathbb{R}} \boldsymbol{\mathcal{E}}(\mathbf{x}, t) e^{i\omega t} \mathrm{d}t,\\ \mathbf{H}(\mathbf{x}) &:= (\mathcal{F}_t \boldsymbol{\mathcal{H}})(\mathbf{x}; \omega) = \int_{\mathbb{R}} \boldsymbol{\mathcal{H}}(\mathbf{x}, t) e^{i\omega t} \mathrm{d}t.\end{aligned}$$

According to $\mathcal{F}_t(u') = -i\omega \mathcal{F}_t u$, further applying the Fourier transform operator to equations (2.1a)-(2.1d) , we get the time harmonic Maxwell equations:

$$\nabla \times \mathbf{E}(\mathbf{x}) - i\omega \mu_0 \mathbf{H}(\mathbf{x}) = 0, \tag{2.2a}$$

$$\nabla \times \mathbf{H}(\mathbf{x}) + i\omega \epsilon_0 \epsilon(\mathbf{x}) \mathbf{E}(\mathbf{x}) = 0, \tag{2.2b}$$

$$\nabla \cdot (\epsilon(\mathbf{x}) \mathbf{E}(\mathbf{x})) = 0, \tag{2.2c}$$

$$\nabla \cdot \mathbf{H}(\mathbf{x}) = 0. \tag{2.2d}$$

Remark 2.1. *Since the Fourier transformation forms complex-valued fields, we should remember to take the real part of the above equations to obtain the physical fields.*

Now applying the curl operator to (2.2a) and using (2.2b), we obtain

$$\nabla \times (\nabla \times \mathbf{E}(\mathbf{x})) - (\frac{\omega}{c})^2 \epsilon(\mathbf{x}) \mathbf{E}(\mathbf{x}) = 0, \tag{2.3}$$

where $\epsilon_0\mu_0 = c^{-2}$. Similarly, applying the curl operator to (2.2b) and using (2.2a), we obtain

$$\nabla \times \left(\left(\frac{1}{\epsilon(\mathbf{x})} \right) \nabla \times \mathbf{H}(\mathbf{x}) \right) - \left(\frac{\omega}{c} \right)^2 \mathbf{H}(\mathbf{x}) = 0. \tag{2.4}$$

For a given frequency ω, we can find the existence of the spatial pattern $\mathbf{E}(\mathbf{x})$ and $\mathbf{H}(\mathbf{x})$ through the above equations (2.3) and (2.4). In fact, we only need to consider one of the above equations, since we can derive from (2.2a) and (2.2b) that

$$\mathbf{H}(\mathbf{x}) = -\frac{i}{\omega\mu_0} \nabla \times \mathbf{E}(\mathbf{x}), \tag{2.5a}$$

$$\mathbf{E}(\mathbf{x}) = \frac{i}{\omega\epsilon_0\epsilon(\mathbf{x})} \nabla \times \mathbf{H}(\mathbf{x}). \tag{2.5b}$$

Remark 2.2. *The two divergence equations (2.2c) and (2.2d) are implicitly satisfied, which can easily be seen by applying the divergence operator to equations (2.2a) and (2.2b), and considering the fact that $\omega > 0$. Hence, now we only focus on the other two of the time harmonic Maxwell equations as long as we drop those "spurious modes" existing at $\omega = 0$.*

To summarize, the eigenvalue problems (2.3) and (2.4) are two crucial parts of studying the propagation of electromagnetic waves in PhCs and our aim is to find the eigenpairs $(\omega, \mathbf{E})$ and $(\omega, \mathbf{H})$ satisfying these two equations, respectively.

2.1 Modes in two-dimensional Photonic Crystals

In 2D case, the permittivity ϵ is invariant in the direction of the holes or rods, the z-direction. Hence, the permittivity ϵ satisfies $\epsilon(\mathbf{x}) = \epsilon(x, y, 0)$, for all $\mathbf{x} = (x, y, z) \in \mathbb{R}^3$. So we can also restrict our electric field and magnetic field to the xy plane, i.e.,

$$\mathbf{E}(\mathbf{x}) = \mathbf{E}(x, y, 0) = (E_1(x, y, 0), E_2(x, y, 0), E_3(x, y, 0)),$$
$$\mathbf{H}(\mathbf{x}) = \mathbf{H}(x, y, 0) = (H_1(x, y, 0), H_2(x, y, 0), H_3(x, y, 0)),$$

for all $\mathbf{x} = (x, y, z) \in \mathbb{R}^3$. Then a straightforward calculation leads to

$$\nabla \times \mathbf{E} = \left(\frac{\partial E_3}{\partial y} \right) \mathbf{i} + \left(-\frac{\partial E_3}{\partial x} \right) \mathbf{j} + \left(\frac{\partial E_2}{\partial x} - \frac{\partial E_1}{\partial y} \right) \mathbf{k}, \tag{2.6}$$

$$\nabla \times (\nabla \times \mathbf{E}) = \left(\frac{\partial^2 E_2}{\partial y \partial x} - \frac{\partial^2 E_1}{\partial y^2} \right) \mathbf{i} + \left(-\frac{\partial^2 E_2}{\partial x^2} + \frac{\partial^2 E_1}{\partial x \partial y} \right) \mathbf{j} + \left(-\frac{\partial^2 E_3}{\partial x^2} - \frac{\partial^2 E_3}{\partial y^2} \right) \mathbf{k}, \tag{2.7}$$

$$\nabla \times \mathbf{H} = \left(\frac{\partial H_3}{\partial y} \right) \mathbf{i} + \left(-\frac{\partial H_3}{\partial x} \right) \mathbf{j} + \left(\frac{\partial H_2}{\partial x} - \frac{\partial H_1}{\partial y} \right) \mathbf{k}, \tag{2.8}$$

$$\nabla \times \left(\frac{1}{\epsilon(\mathbf{x})} \nabla \times \mathbf{H} \right) = \left(\frac{\partial}{\partial y} \frac{1}{\epsilon(\mathbf{x})} \frac{\partial H_2}{\partial x} - \frac{\partial}{\partial y} \frac{1}{\epsilon(\mathbf{x})} \frac{\partial H_1}{\partial y} \right) \mathbf{i} + \left(-\frac{\partial}{\partial x} \frac{1}{\epsilon(\mathbf{x})} \frac{\partial H_2}{\partial x} + \frac{\partial}{\partial x} \frac{1}{\epsilon(\mathbf{x})} \frac{\partial H_1}{\partial y} \right) \mathbf{j} +$$
$$\left(-\frac{\partial}{\partial x} \frac{1}{\epsilon(\mathbf{x})} \frac{\partial H_3}{\partial x} - \frac{\partial}{\partial y} \frac{1}{\epsilon(\mathbf{x})} \frac{\partial H_3}{\partial y} \right) \mathbf{k}. \tag{2.9}$$

Plugging (2.7) into (2.3), we obtain

$$-\Delta E_3(\mathbf{x}) - (\frac{\omega}{c})^2 \epsilon(\mathbf{x}) E_3(\mathbf{x}) = 0, \quad \text{in } \mathbb{R}^2.$$

Combining with (2.6), (2.5a) implies

$$H_1(\mathbf{x}) = -\frac{i}{\omega\mu_0}\frac{\partial}{\partial y}E_3(\mathbf{x}),$$
$$H_2(\mathbf{x}) = \frac{i}{\omega\mu_0}\frac{\partial}{\partial x}E_3(\mathbf{x}).$$

Analogously, we derive

$$-\nabla\cdot\frac{1}{\epsilon(\mathbf{x})}\nabla H_3(\mathbf{x}) - (\frac{\omega}{c})^2 H_3(\mathbf{x}) = 0, \quad \text{in } \mathbb{R}^2.$$

Following equation (2.8) and (2.5b), we get

$$E_1(\mathbf{x}) = \frac{i}{\omega\epsilon_0\epsilon(\mathbf{x})}\frac{\partial}{\partial y}H_3(\mathbf{x}),$$
$$E_2(\mathbf{x}) = -\frac{i}{\omega\epsilon_0\epsilon(\mathbf{x})}\frac{\partial}{\partial x}H_3(\mathbf{x}).$$

The above derivation yields two scalar eigenvalue problems and we also deduce that the components of the electric field and magnetic field are not independent. Indeed, H_1, H_2 are related to E_3, and E_1, E_2 are related to H_3. Thus, we can classify the electromagnetic waves in terms of whether E_3 or H_3 equals to zero. which is often referred to as TE mode and TM mode respectively. In other words, in TE mode, the magnetic field is directed along the z axis and the electric field is perpendicular to this axis, while TM mode consists of electric field along z axis and magnetic field perpendicular to the z axis.

To conclude, the eigenvalue problems in 2D PhCs reduce to

$$-\Delta E(\mathbf{x}) - (\frac{\omega}{c})^2\epsilon(\mathbf{x})E(\mathbf{x}) = 0, \text{ in } \mathbb{R}^2 \qquad \textbf{(TM mode)}, \tag{2.10}$$
$$-\nabla\cdot\frac{1}{\epsilon(\mathbf{x})}\nabla H(\mathbf{x}) - (\frac{\omega}{c})^2 H(\mathbf{x}) = 0, \text{ in } \mathbb{R}^2 \qquad \textbf{(TE mode)}. \tag{2.11}$$

2.2 Bloch's theorem

Bloch's theorem [22] states that in periodic crystals, wave functions take the form of a plane wave modulated by a periodic function. Mathematically, they can be written as

$$\Psi(\mathbf{x}) = e^{i\mathbf{k}\cdot\mathbf{x}}u(\mathbf{x}),$$

where Ψ is the wave function, $u(\mathbf{x})$ is a periodic function with the same periodicity as the crystal lattice, $\mathbf{k}$ is the wave vector. Functions of this form are known as Bloch functions or Bloch states.

Proposition 2.1. *The periodicity condition of $u(\mathbf{x})$ implies that each Bloch state can be determined by its values within the unit cell Ω spanned by the primitive lattice vectors. So it is sufficient to study only in the unit cell Ω.*

Proposition 2.2. *In 2-dimension case, $e^{i(\mathbf{k}+\mathbf{n}\cdot\mathbf{b})\cdot\mathbf{x}} = e^{i\mathbf{k}\cdot\mathbf{x}}$, where $\mathbf{n} = (n_1, n_2) \in (\mathbb{Z}^+)^2$, $\mathbf{b} = (\mathbf{b}_1, \mathbf{b}_2)$, and each $\mathbf{b}_i$ is the reciprocal lattice vector with the property $\mathbf{b}_i \cdot \mathbf{a}_j = 2\pi\delta_{ij}$ for all primitive lattice vectors $\mathbf{a_j}$. Thus, the wave vector can be restricted into the unit reciprocal lattice $\mathcal{B}$, which is the so-called first Brillouin zone. In addition, note that in some cases, further utilization of symmetry can even restrict $\mathbf{k}$ to the triangular irreducible Brillouin zone $\mathcal{B}_{\text{red}}$ which is proved in detail in [17].*

By Bloch's theorem, we have $E(\mathbf{x}) = e^{i\mathbf{k}\cdot\mathbf{x}}u_1(\mathbf{x})$, $H(\mathbf{x}) = e^{i\mathbf{k}\cdot\mathbf{x}}u_2(\mathbf{x})$, and hence the eigenvalue problems (2.10) and (2.11) reduce to

$$-(\nabla + i\mathbf{k}) \cdot ((\nabla + i\mathbf{k})u_1(\mathbf{x})) - (\frac{\omega}{c})^2\epsilon(\mathbf{x})u_1(\mathbf{x}) = 0, \text{ in } \Omega \qquad \textbf{(TM mode)}, \tag{2.12a}$$

$$-(\nabla + i\mathbf{k}) \cdot \left(\frac{1}{\epsilon(\mathbf{x})}(\nabla + i\mathbf{k})u_2(\mathbf{x})\right) - (\frac{\omega}{c})^2 u_2(\mathbf{x}) = 0, \text{ in } \Omega \qquad \textbf{(TE mode)}, \tag{2.12b}$$

where $\mathbf{k}$ varies in the first Brillouin zone, and $u_i(\mathbf{x})$ satisfies the periodic boundary conditions $u_i(\mathbf{x}) = u_i(\mathbf{x} + \mathbf{a_j})$ with $\mathbf{a_j}$ being the primitive lattice vector for $i, j = 1, 2$.

Now we consider both modes simultaneously by

$$-(\nabla + i\mathbf{k}) \cdot \alpha(\mathbf{x})(\nabla + i\mathbf{k})u(\mathbf{x}) - \lambda\beta(\mathbf{x})u(\mathbf{x}) = 0, \quad \text{in } \Omega, \tag{2.13}$$

with $\mathbf{k} \in \mathcal{B}$ and $\lambda = \left(\frac{\omega}{c}\right)^2$. In the TM mode, U describes the electric field E in z-direction and the coefficients $\alpha(\mathbf{x})$ and $\beta(\mathbf{x})$ are

$$\alpha(\mathbf{x}) := 1, \quad \beta(\mathbf{x}) := \epsilon(\mathbf{x}).$$

Similarly, in the TE mode, U describes the magnetic field H in z-direction and the coefficients $\alpha(\mathbf{x})$ and $\beta(\mathbf{x})$ are

$$\alpha(\mathbf{x}) := \frac{1}{\epsilon(\mathbf{x})}, \quad \beta(\mathbf{x}) := 1.$$

3 Regularity of band functions and eigenfunctions

To further analyze the properties of band functions, we first define some function spaces. Let $L^2(\Omega)$ denote the space of square integrable functions equipped with the weighted norm

$$\|f\|^2 := \int_\Omega |f(\mathbf{x})|^2\beta(\mathbf{x})\mathrm{d}\mathbf{x}.$$

Let $H^1(\Omega) \subset L^2(\Omega)$ with square integrable gradient be equipped with the standard H^1 norm. $H^1_\pi(\Omega) \subset H^1(\Omega)$ is composed of functions with periodic boundary conditions on $\partial\Omega$. Moreover, let

$$H^1_\pi(\Omega, \Delta, \alpha) := \left\{v \in H^1_\pi(\Omega) : \Delta v \in L^2(\Omega), \alpha\partial_{\mathbf{n}_L} v|_L = -\alpha\partial_{\mathbf{n}_R} v|_R \text{ and } \alpha\partial_{\mathbf{n}_T} u|_T = -\alpha\partial_{\mathbf{n}_B} u|_B\right\}$$

with $\partial_{\mathbf{n}_L}, \partial_{\mathbf{n}_R}, \partial_{\mathbf{n}_B}, \partial_{\mathbf{n}_T}$ denoting the outward normal derivatives on the left, right, bottom and top boundaries of Ω, respectively.

The Bloch's theorem expands the original operator $\mathcal{L} := -\frac{1}{\beta(\mathbf{x})}\nabla \cdot \alpha(\mathbf{x})\nabla$ defined on Sobolev space $H^2(\mathbb{R}^2)$ into a new set of operators $\mathcal{L}_\mathbf{k} := -\frac{1}{\beta(\mathbf{x})}(\nabla + i\mathbf{k}) \cdot \alpha(\mathbf{x})(\nabla + i\mathbf{k})$ defined on $H^1_\pi(\Omega, \Delta, \alpha)$. The following theorem proved in [10] represents the spectrum of the operator $\mathcal{L}$ using that of $\mathcal{L}_\mathbf{k}$.

Theorem 3.1. *For all $\mathbf{k} \in \mathcal{B}$, $\mathcal{L}_\mathbf{k}$ has a non-negative discrete spectrum. We can enumerate these eigenvalues in a nondecreasing manner and repeat according to their finite multiplicities as*

$$0 \leqslant \lambda_1(\mathbf{k}) \leqslant \lambda_2(\mathbf{k}) \leqslant \cdots \leqslant \lambda_n(\mathbf{k}) \leqslant \cdots \leqslant \infty.$$

$\{\lambda_n(\mathbf{k})\}_{n=1}^{\infty}$ is an infinite sequence with $\lambda_n(\mathbf{k})$ being a continuous function with respect to the wave vector $\mathbf{k}$ and $\lambda_n(\mathbf{k}) \to \infty$ when $n \to \infty$. Moreover, the spectrum $\sigma(\mathcal{L})$ of the operator $\mathcal{L}$ is connected to the spectrum $\sigma(\mathcal{L}_{\mathbf{k}})$ of the operators $\mathcal{L}_{\mathbf{k}}$ through

$$\sigma(\mathcal{L}) = \bigcup_{\mathbf{k}\in\mathcal{B}} \sigma(\mathcal{L}_{\mathbf{k}}).$$

In view that $\lambda_n(\mathbf{k}) = \left(\frac{\omega_n(\mathbf{k})}{c}\right)^2$, Theorem 3.1 implies that each band function $\omega_n(\mathbf{k})$ is continuous for all band number $n \in \mathbb{N}^+$.

Next we introduce one of the most important properties of band functions, which lays the main foundation for our proposed interpolation method.

Theorem 3.2 (Piecewise analyticity of the band functions)**.** *2D periodic PhCs band functions are piecewise analytic in the first Brillouin zone $\mathcal{B}$. In specific, each band function $\omega_n(\mathbf{k})$ is analytic in $\mathcal{B}\backslash X_n$, where X_n is a subset composed of branch points and the origin with zero Lebesgue measure.*

Proof. Our proof is mainly based upon the analyticity of the Bloch variety that was proved in [24, Theorem 4.4.2]. For the sake of completeness, we repeat it in Theorem 3.3. Our proof is inspired by the procedure used in [36], wherein the Bloch wave of Schrödinger equation with periodic potential was considered.

The Bloch variety is defined as

$$B(\mathcal{L}_{\mathbf{k}}) = \left\{(\mathbf{k},\lambda) \in \mathbb{R}^3 : \mathcal{L}_{\mathbf{k}}u = \lambda u \text{ admits a nonzero function } u \in H^1_{\pi}(\Omega,\Delta,\alpha)\right\}. \tag{3.1}$$

Theorem 3.3 implies that there is an analytic function $D(\mathbf{k},\lambda)$ on $\mathbb{R}^3$ such that $B(\mathcal{L}_{\mathbf{k}})$ is its set of zeros, i.e.,

$$B(\mathcal{L}_{\mathbf{k}}) = \left\{(\mathbf{k},\lambda) \in \mathbb{R}^3 | D(\mathbf{k},\lambda) = 0\right\}.$$

We now decompose $B(\mathcal{L}_{\mathbf{k}})$ into two types of sets, where the first type is

$$\begin{aligned} B^r := \Big\{(\mathbf{k}_0,\lambda_0) \in B(\mathcal{L}_{\mathbf{k}}) : &\frac{\partial^{m-1} D}{\partial \lambda^{m-1}} = 0 \text{ in a neighborhood of } (\mathbf{k}_0,\lambda_0) \\ &\text{and } \frac{\partial^m D}{\partial \lambda^m}|_{(\mathbf{k}_0,\lambda_0)} \neq 0 \text{ for some } m \in \mathbb{N}^+\Big\}, \end{aligned} \tag{3.2}$$

and the second type is $B^s := B(\mathcal{L}_{\mathbf{k}})\backslash B^r$.

Note that $\lambda_n(\mathbf{k}) \to \infty$ when $n \to \infty$ for all $\mathbf{k} \in \mathcal{B}$. To the aim of defining a bounded subset of $B(\mathcal{L}_{\mathbf{k}})$, we introduce

$$B_n := \bigcup_{l=1}^{n} \{(\mathbf{k},\lambda_l(\mathbf{k}))|(\mathbf{k},\lambda_l(\mathbf{k})) \in B(\mathcal{L}_{\mathbf{k}})\}.$$

Analogously, this leads to bounded subsets of B^r and B^s given by

$$B_n^r := B_n \cap B^r \quad \text{and} \quad B_n^s := B_n \cap B^s.$$

Furthermore, let X_n^s be the projection of B_n^s onto $\lambda = 0$ defined by

$$X_n^s := \{\mathbf{k} \in \mathcal{B} | (\mathbf{k},\lambda) \in B_n^s \text{ for some } \lambda\}.$$

The definition of B_n^s implies that X_n^s is the set of branch points for the first n bands. Moreover, for any $(\mathbf{k}_0, \lambda_0) \in B_n^s$, there is an integer $m \in \mathbb{N}^+$ such that $(\mathbf{k}_0, \lambda_0) \in \{(\mathbf{k}, \lambda) : D(\mathbf{k}, \lambda) = 0\} \cap \{(\mathbf{k}, \lambda) : \frac{\partial^m D}{\partial \lambda^m} = 0\}$, which is a one-dimensional variety. Hence X_n^s, the projection of B_n^s onto the hyperplane $\lambda = 0$, is a subset of $\mathcal{B}$ with Lebesgue measure zero. Let $\mathbf{k}_0 \in \mathcal{B} \backslash X_n^s$, i.e., $(\mathbf{k}_0, \lambda_l(\mathbf{k}_0)) \in B_n^r$ for $l = 1, \cdots, n$. Due to the implicit mapping theorem for analytic functions [21], there is a neighborhood $N(\mathbf{k}_0)$ in which $\lambda_l(\mathbf{k})$ is the unique analytic solution of $\frac{\partial^{m-1} D}{\partial \lambda^{m-1}} = 0$ for some $m \in \mathbb{N}^+$. This implies that each positive band function $\omega_l(\mathbf{k}) = c \cdot \sqrt{\lambda_l(\mathbf{k})}$ is analytic in $\mathcal{B} \backslash X_n^s$. Besides, it is well known that only at the origin the first eigenvalue equals to 0. Thus, we have $X_n = X_n^s \cup \{\mathbf{0}\}$. □

Theorem 3.3. ([24, Theorem 4.4.2]) *Let L be a general periodic elliptic operator in $\mathbb{R}^n$, then the complex Bloch variety of L,*

$$B(L) = \{(\mathbf{k}, \lambda) \in \mathbb{C}^n \times \mathbb{C} | \text{ the equation } Lu = \lambda u \text{ has a non-zero Bloch function with } \mathbf{k}\},$$

is the set of all zeros of an entire function on $\mathbb{C}^{n+1}$.

Theorem 3.4 (mentioned in [23] and proved by perturbation theory [20])**.** *If we only consider one component k_i of the vector $\mathbf{k} = (k_1, k_2)$, then all the positive band functions can be resorted when crossing the branch points such that they are analytic functions with respect to k_i.*

Theorem 3.2 states that band functions are piecewise analytic with potential singularities occurring at branch points and origin. Theorem 3.4 further shows the analytic continuation of band functions in one variable through branch points. In the following, we will discuss the properties of these singular points and the smoothness of band functions in more details. First we study the limit of eigenfunctions along any band functions.

The variational formulation of (2.13) is: for a given $\mathbf{k} \in \mathcal{B}$, find non-trivial eigenpair $(\lambda, u) \in (\mathbb{R}, H_\pi^1(\Omega))$ satisfying

$$\begin{cases} \int_\Omega \alpha(\nabla + i\mathbf{k})u \cdot (\nabla - i\mathbf{k})\bar{v} - \lambda\beta u\bar{v}\mathrm{d}x = 0, \text{ for all } v \in H_\pi^1(\Omega) \\ \|u\| = 1. \end{cases} \tag{3.3}$$

Using the sesquilinear forms

$$\begin{aligned} a(u, v) &:= \int_\Omega \alpha(\nabla + i\mathbf{k})u \cdot (\nabla - i\mathbf{k})\bar{v}\, \mathrm{d}x, \\ b(u, v) &:= \int_\Omega \beta u\bar{v}\, \mathrm{d}x, \end{aligned}$$

(3.3) reads: for a given $\mathbf{k}$ in $\mathcal{B}$, find non-trivial eigenpair $(\lambda, u) \in (\mathbb{R}, H_\pi^1(\Omega))$ such that

$$\begin{cases} a(u, v) = \lambda b(u, v), \text{ for all } v \in H_\pi^1(\Omega) \\ b(u, u) = 1. \end{cases} \tag{3.4}$$

Suppose that we fix a particular $\mathbf{k}$, then we denote the eigenspace of one of the corresponding eigenvalues λ as $E(\lambda)$ and let $\tilde{\mathcal{L}}_\mathbf{k}$ be the operator defined on the quotient space $\tilde{H}_\pi^1(\Omega, \Delta, \alpha) := H_\pi^1(\Omega, \Delta, \alpha)/E(\lambda)$ with the same form as $\mathcal{L}_\mathbf{k}$. Then the unique different value between the resolvent sets of $\tilde{\mathcal{L}}_\mathbf{k}$ and $\mathcal{L}_\mathbf{k}$ is λ. More precisely, they have the relation $\rho(\tilde{\mathcal{L}}_\mathbf{k}) = \rho(\mathcal{L}_\mathbf{k}) \cup \{\lambda\}$, i.e., λ is in the resolvent set of $\tilde{\mathcal{L}}_\mathbf{k}$. In the following, we investigate the regularity of the eigenfunctions.

Theorem 3.5 (Continuity of the eigenfunctions in $\mathcal{B}\backslash X_n$). *Let $\omega_n(\mathbf{k})$ be the nth band function for $n \in \mathbb{N}^+$, and let $u(x;\mathbf{k})$ be one of its corresponding normalized eigenfunctions if the corresponding eigenvalue $\lambda_n(\mathbf{k})$ has multiplicity larger than one, then the follow statement hold,*

(i) $u(x;\mathbf{k})$ can be defined such that $u(x;\mathbf{k})$ is continuous with respect to the wave vector $\mathbf{k}$ for $\mathbf{k} \notin X_n$.

(ii) If $\mathbf{k} \in X_n$ and the multiplicity of the eigenvalue $\lambda_n(\mathbf{k})$ is $M \geqslant 2$ with $\{u_q(\mathbf{x};\mathbf{k})\}_{q=1}^M$ being its associated eigenfunctions, then there may be a normalized eigenfunction $u(x;\mathbf{k})$ that admits jump discontinuity, i.e., there is $\{c_{i\pm}^q\}_{q=1}^M \subset \mathbb{C}$, satisfying

$$\lim_{\delta\to 0} u(\mathbf{x};\mathbf{k}\pm\delta\mathbf{e}_i) = \sum_{q=1}^M c_{i\pm}^q u_q(\mathbf{x};\mathbf{k}) \text{ and } \left\|\sum_{q=1}^M c_{i\pm}^q u_q(\mathbf{x};\mathbf{k})\right\| = 1,$$
$$\text{but } \sum_{q=1}^M c_{i+}^q u_q(\mathbf{x};\mathbf{k}) \neq \sum_{q=1}^M c_{i-}^q u_q(\mathbf{x};\mathbf{k}).$$

Here, $\delta > 0$ is a parameter such that $\mathbf{k}\pm\delta\mathbf{e}_i \in \mathcal{B}$ and $\mathbf{e}_i$ is the canonical basis in $\mathbb{R}^2$ for $i = 1, 2$.

Proof. For the sake of simplicity, we drop the band number for the moment. Let $\omega(\mathbf{k})$ be the band function with $u(\mathbf{x};\mathbf{k})$ being the associated eigenfunction for any $\mathbf{k} \in \mathcal{B}$. Let the error function be

$$e_i(\delta) := u(\mathbf{x};\mathbf{k}+\delta\mathbf{e}_i) - u(\mathbf{x};\mathbf{k}),$$

with $\delta > 0$ being a parameter such that $\mathbf{k}+\delta\mathbf{e}_i \in \mathcal{B}$.

By an application of (2.13) and (3.4), we deduce that the error function $e_i(\delta)$ satisfies the strong formulation

$$(\mathcal{L}_\mathbf{k} - \lambda(\mathbf{k}))\, e_i(\delta) = f(\mathbf{x};\delta), \tag{3.5}$$

where

$$\begin{aligned} f(\mathbf{x};\delta) = {} & (\lambda(\mathbf{k}+\delta\mathbf{e}_i) - \lambda(\mathbf{k}))\, u(\mathbf{x};\mathbf{k}+\delta\mathbf{e}_i) - \delta(2k_i+\delta)\frac{1}{\epsilon(\mathbf{x})} u(\mathbf{x};\mathbf{k}+\delta\mathbf{e}_i) \\ & + \delta i \frac{1}{\beta(\mathbf{x})}\frac{\partial}{\partial x_i}\left(\alpha(\mathbf{x}) u(\mathbf{x};\mathbf{k}+\delta\mathbf{e}_i)\right) + \delta i \frac{1}{\epsilon(\mathbf{x})}\frac{\partial}{\partial x_i} u(\mathbf{x};\mathbf{k}+\delta\mathbf{e}_i). \end{aligned}$$

The corresponding weak formulation is

$$a(e_i(\delta), v) - \lambda(\mathbf{k}) b(e_i(\delta), v) = g(v;\mathbf{k},\lambda,u), \text{ for all } v \in H^1_\pi(\Omega),$$

with $g(v;\mathbf{k},\lambda,u)$ being

$$\begin{aligned} g(v;\mathbf{k},\lambda,u) = {} & (\lambda(\mathbf{k}+\delta\mathbf{e}_i) - \lambda(\mathbf{k}))\, b(u(\mathbf{x};\mathbf{k}+\delta\mathbf{e}_i), v) \\ & - \delta(2k_i+\delta) m_\alpha(u(\mathbf{x};\mathbf{k}+\delta\mathbf{e}_i), v) - \delta m_{\alpha i}(u(\mathbf{x};\mathbf{k}+\delta\mathbf{e}_i), v), \end{aligned}$$

and

$$m_{\alpha i}(u,v) = \int_\Omega i\alpha\left(u\frac{\partial\bar{v}}{\partial x_i} - \bar{v}\frac{\partial u}{\partial x_i}\right)\mathrm{d}\mathbf{x}, \quad i = 1, 2, \tag{3.6a}$$

$$m_\alpha(u,v) = \int_\Omega \alpha u\bar{v}\,\mathrm{d}\mathbf{x}. \tag{3.6b}$$

Following the Fredholm–Riesz–Schauder theory [29], we can derive that for a given $\mathbf{k}$ and a corresponding eigenvalue $\lambda(\mathbf{k})$, Problem (3.5) has a unique solution $e_i(\delta) = (\tilde{\mathcal{L}}_{\mathbf{k}} - \lambda\mathbf{I})^{-1} f(\mathbf{x};\delta)$ in the quotient space $\tilde{H}^1_\pi(\Omega,\Delta,\alpha)$ which is bounded by

$$\|e_i(\delta)\|_{\tilde{H}^1_\pi(\Omega)} \leqslant \|(\tilde{\mathcal{L}}_{\mathbf{k}} - \lambda\mathbf{I})^{-1}\| \cdot \|f(\mathbf{x};\delta)\|. \tag{3.7}$$

Note that $\lambda(\mathbf{k})$ is a continuous function and $u(\mathbf{x};\mathbf{k}) \in H^1_\pi(\Omega,\Delta,\alpha)$, which lead to $\|f(\mathbf{x};\delta)\| \to 0$ as $\delta \to 0$. Together with (3.7), the error function $e_i(\delta)$ converges to some function in $E(\lambda(\mathbf{k}))$ as $\delta \to 0$. In a similar manner, we obtain $u(\mathbf{x};\mathbf{k}-\delta\mathbf{e}_i) - u(\mathbf{x};\mathbf{k})$ converges to some function in $E(\lambda(\mathbf{k}))$ as $\delta \to 0$, i.e.,

$$\lim_{\delta\to 0} u(\mathbf{x};\mathbf{k}\pm\delta\mathbf{e}_i) \in E(\lambda(\mathbf{k})). \tag{3.8}$$

Next, we discuss case by case whether a given wave vector $\mathbf{k}$ belongs to the singular set X_n as defined in Theorem 3.2. If $\mathbf{k} \notin X_n$ and the multiplicity of λ is $1 \leqslant M \in \mathbb{N}^+$, then the definition of B^r (3.2) implies the existence of a neighborhood $N(\mathbf{k})$ such that for any $\mathbf{k}\pm\delta\mathbf{e}_i \in N(\mathbf{k})$, the eigenvalues $\lambda(\mathbf{k}\pm\delta\mathbf{e}_i)$ have the same multiplicity. Together with (3.8), this implies the corresponding eigenfunction satisfying

$$\begin{aligned}
&\lim_{\delta\to 0} u(\mathbf{x};\mathbf{k}\pm\delta\mathbf{e}_i) = \sum_{q=1}^{M} c^q_{i\pm} u_q(\mathbf{x};\mathbf{k}),\\
&\left\| \sum_{q=1}^{M} c^q_{i\pm} u_q(\mathbf{x};\mathbf{k}) \right\| = 1.
\end{aligned}$$

Here, $\{c^q_{i\pm}\}_{q=1}^M \subset \mathbb{C}$ are some constant. Thus, we can always find a combination of these M normalized eigenfunctions $\{u_q(\mathbf{x};\mathbf{k})\}_{q=1}^M$ such that there is a normalized eigenfunction $u(\mathbf{x};\mathbf{k})$, satisfying

$$\lim_{\delta\to 0} u(\mathbf{x};\mathbf{k}+\delta\mathbf{e}_i) = \lim_{\delta\to 0} u(\mathbf{x};\mathbf{k}-\delta\mathbf{e}_i) = u(\mathbf{x};\mathbf{k}), \qquad \text{for } i = 1,2.$$

When $\mathbf{k} \in X_n$ is a singular point and $\lambda(\mathbf{k})$ has multiplicity $M \geqslant 2$, there is no such kind of neighborhood $N(\mathbf{k})$ such that for any $\mathbf{k}\pm\delta\mathbf{e}_i \in N(\mathbf{k})$, the multiplicity of $\lambda(\mathbf{k}\pm\delta\mathbf{e}_i)$ is also M since the Lebesgue measure of X_n vanishes. Consequently, there is no guarantee we can construct such kind of normalized eigenfunctions to ensure the continuity at $\mathbf{k}$. We only have for any normalized eigenfunction $u(\mathbf{x};\mathbf{k}\pm\delta\mathbf{e}_i)$ at $\mathbf{k}\pm\delta\mathbf{e}_i$,

$$\lim_{\delta\to 0} u(\mathbf{x};\mathbf{k}\pm\delta\mathbf{e}_i) = \sum_{q=1}^{M} c^q_{i\pm} u_q(\mathbf{x};\mathbf{k}),$$

with some constant $\{c^q_{i\pm}\}_{q=1}^M \subset \mathbb{C}$ such that $\|\sum_{q=1}^M c^q_{i\pm} u_q(\mathbf{x};\mathbf{k})\| = 1$ for $i = 1,2$. This completes the proof. □

Remark 3.1 (Differentiability of the eigenfunctions in $\mathcal{B}\backslash X_n$)**.** *As is shown in [23], we can further prove that the eigenfunctions corresponding to the nth band function can indeed be organized to be continuously differentiable of any degree in $\mathcal{B}\backslash X_n$. However, the properties of eigenfunctions at X_n are not discussed in the aforementioned paper. The authors conjectured that there may exist an ordering of band functions such that the corresponding eigenfunctions are also continuously differentiable at X_n. In contrast, Theorem 3.5 indicates the possibility of discontinuity of the eigenfunctions in X_n.*

Now, we are able to prove the regularity of band functions.

Theorem 3.6 (Lipschitz continuity of the band functions)**.** *For the case of 2-dimension periodic PhCs, $\omega_n(\mathbf{k}) \in Lip(\mathcal{B}) \cap \mathring{A}(\mathcal{B})$ for all $n \in \mathbb{N}^+$. Here, $Lip(\mathcal{B})$ is the space of Lipschitz continuous functions in the first Brillouin zone $\mathcal{B}$ and $\mathring{A}(\mathcal{B})$ denotes the space composed of piecewise analytic functions with their singular point sets having a zero Lebesgue measure.*

Proof. On the one hand, let $\mathbf{k} \in \mathcal{B} \backslash X_n$, and suppose the multiplicity of the eigenvalue $\lambda_n(\mathbf{k})$ is $M \geqslant 1$ for some $n \in \mathbb{N}^+$. For simplicity, we drop n and $\mathbf{k}$ in the proof. Theorem 3.5 guarantees the existence of a normalized eigenfunction $u(\mathbf{x}; \mathbf{k})$ which is continuous in a neighborhood of $\mathbf{k}$. Taking the partial derivative with respect to k_i for $i = 1, 2$ at $\mathbf{k}$ on both sides of (3.4), this leads to

$$a(\frac{\partial u}{\partial k_i}, v) - \lambda b(\frac{\partial u}{\partial k_i}, v) = f^{(1)}(v; \mathbf{k}, u, \frac{\partial \lambda}{\partial k_i}),$$

with

$$f^{(1)}(v; \mathbf{k}, u, \frac{\partial \lambda}{\partial k_i}) := -m_{\alpha i}(u, v) - 2k_i m_\alpha(u, v) + \frac{\partial \lambda}{\partial k_i} b(u, v).$$

Here, the bilinear forms $m_{\alpha i}(\cdot, \cdot)$ and $m_\alpha(\cdot, \cdot)$ are defined in (3.6).

Note that the operator in the equation above $(\mathcal{L}_k - \lambda \mathbf{I})$ has the eigenspace $E(\lambda)$ as its kernel. Let $\{u_p\}_{p=1}^M$ be a set of basis in $E(\lambda)$. As a consequence of the Fredholm–Riesz–Schauder theory [29], adding additional orthogonality with $E(\lambda)$ leads to the well-posedness of the following problem: seeking $\partial_{k_i} u \in H^1_\pi(\Omega)$, s.t.,

$$\begin{cases} a(\partial_{k_i} u, v) - \lambda b(\partial_{k_i} u, v) = f^{(1)}(v; \mathbf{k}, u, \dfrac{\partial \lambda}{\partial k_i}) & \text{for all } v \in H^1_\pi(\Omega), \\ b(\partial_{k_i} u, u_p) = 0 & \text{for } p = 1, \cdots, M. \end{cases} \tag{3.9}$$

Let the test function $v := u$, we obtain

$$a(\partial_{k_i} u, u) - \lambda b(\partial_{k_i} u, u) = \overline{a(u, \partial_{k_i} u) - \lambda b(u, \partial_{k_i} u)} = f^{(1)}(u; \mathbf{k}, u, \frac{\partial \lambda}{\partial k_i}) = 0. \tag{3.10}$$

Therefore, $\frac{\partial \lambda}{\partial k_i}$ has to be the solution to the following problem,

$$f^{(1)}(u; \mathbf{k}, u, \frac{\partial \lambda}{\partial k_i}) = 0.$$

This results in

$$\frac{\partial \lambda}{\partial k_i} = 2k_i m_\alpha(u, u) + m_{\alpha i}(u, u). \tag{3.11}$$

Consequently, $\frac{\partial \lambda}{\partial k_i}$ is uniformly bounded.

On the other hand, let $\mathbf{k}_0 \in X_n$ and suppose the multiplicity of the eigenvalue $\lambda_n(\mathbf{k_0})$ is $M \geqslant 1$ for some $n \in \mathbb{N}^+$ and let its associated eigenfunctions be $\{u_q(\mathbf{x}; \mathbf{k}_0)\}_{q=1}^M$. Then a combination of (3.11) and Theorem 3.5 leads to the left and right partial derivatives,

$$\begin{aligned} \frac{\partial \lambda}{\partial {k_i}^\pm}\bigg|_{\mathbf{k}=\mathbf{k}_0} &= \lim_{\delta \to 0^\pm} \left(2k_i m_\alpha(u, u) + m_{\alpha i}(u, u)\right)|_{\mathbf{k}=\mathbf{k}_0+\delta \mathbf{e}_i} \\ &= 2k_i \sum_{q=1}^M \sum_{p=1}^M c_{i\pm}^q c_{i\pm}^p \left(m_\alpha(u_q(\mathbf{x}; \mathbf{k}), u_p(\mathbf{x}; \mathbf{k})) + m_{\alpha i}(u_q(\mathbf{x}; \mathbf{k}), u_p(\mathbf{x}; \mathbf{k}))\right). \end{aligned}$$

Here, the complex values $\{c_{i\pm}^q\}_{q=1}^M \subset \mathbb{C}$ satisfy Theorem 3.5 for $i = 1, 2$. Consequently, $\frac{\partial\lambda}{\partial k_i^{\pm}}\Big|_{\mathbf{k}=\mathbf{k}_0}$ are bounded but may take different values.

Finally, the first partial derivative of each positive band function at $\mathbf{k} \in \mathcal{B}\backslash X_n$ can be easily derived from the relation $\lambda(\mathbf{k}) = \left(\frac{\omega(\mathbf{k})}{c}\right)^2$. Since the first band function vanishes at $\mathbf{k} = 0$, $\frac{\partial\omega_1}{\partial {k_i}^+}\Big|_{\mathbf{k}=0} = \infty$, which is unbounded. Consequently, we proved $\omega_n(\mathbf{k}) \in Lip(\mathcal{B}) \cap \mathring{A}(\mathcal{B})$ for all $n \in \mathbb{N}^+$, and this completes our proof. □

4 Numerical schemes

As shown in the previous section, band functions of 2D periodic PhCs are real-valued, non-negative, continuous, and piecewise analytic within the first Brillouin zone $\mathcal{B}$. Besides, in 2D PhCs with symmetrical structures, there exists a triangular area within the first Brillouin zone $\mathcal{B}$, which is the so-called irreducible Brillouin zone (IBZ) $\mathcal{B}_{\text{red}}$. All other points in $\mathcal{B}$ can be transferred into $\mathcal{B}_{\text{red}}$ by mirror symmetry or rotational symmetry, so the eigenvalues at these points are also the same as the eigenvalues of the corresponding points in $\mathcal{B}_{\text{red}}$, as proved in [17]. Hence, what we focus on is the band function approximation within the triangular domain $\mathcal{B}_{\text{red}}$ or within the quadrilateral domain including $\mathcal{B}_{\text{red}}$ and its mirror symmetric area along one of its edges which we denote as $\tilde{\mathcal{B}}_{\text{red}}$. After we have obtained the approximate band functions in $\mathcal{B}_{\text{red}}$ or $\tilde{\mathcal{B}}_{\text{red}}$, the symmetry allows us to directly acquire the approximate band functions in $\mathcal{B}$.

Based upon the properties of band functions we derived, we exploit in this work the band function reconstruction using Lagrange interpolation. In specific, given a set of N distinct sampling points $\{\mathbf{k}_i\}_{i=1}^N \subset \mathcal{C}$ for $\mathcal{C} := \mathcal{B}_{\text{red}}$ or $\mathcal{C} := \tilde{\mathcal{B}}_{\text{red}}$ and the corresponding band function values $\{\omega(\mathbf{k}_i)\}_{i=1}^N$ for a certain band number, the corresponding Lagrange interpolation $\mathbf{L}\omega$ is a linear combination of the Lagrange polynomials $\{l_i(\mathbf{k})\}_{i=1}^N$ for those sampling points satisfying $l_i(\mathbf{k_j}) = \delta_{ij}$ such that it interpolates the data, i.e.,

$$\mathbf{L}\omega = \sum_{i=1}^{N} \omega(\mathbf{k}_i) l_i(\mathbf{k}). \tag{4.1}$$

We refer to [5, Section 2] for more details on Lagrange interpolation. Here, $\{\omega(\mathbf{k}_i)\}_{i=1}^N$ are derived by solving the eigenvalue problem (2.13) numerically.

As is known that the optimal nodal set within a domain $\mathcal{C}$ in uniform norm is characterized by minimizing the so-called Lebesgue constant $\Gamma_N\left(\{\mathbf{k}_i\}_{i=1}^N\right)$, defined by

$$\Gamma_N(\{\mathbf{k}_i\}_{i=1}^N) := \max_{\mathbf{k}\in\mathcal{C}} \sum_{i=1}^{N} |l_i(\mathbf{k})|. \tag{4.2}$$

Let $P_n(\mathcal{C})$ be the polynomial space with degree at most n such that $N := \dim(P_n(T))$ satisfies $N = (n+1)^2$ for $\mathcal{C} = \tilde{\mathcal{B}}_{red}$ and $N = \frac{1}{2}(n+1)(n+2)$ for $\mathcal{C} = \mathcal{B}_{red}$. Then we have the following near-best approximation which bounds our interpolation error through the Lebesgue constant [34, Theorem 15.1],

$$\sup_{\mathbf{k}\in\mathcal{C}} |\omega(\mathbf{k}) - \mathbf{L}\omega(\mathbf{k})| \leqslant \left(1 + \Gamma_N\left(\{\mathbf{k}_i\}_{i=1}^N\right)\right) \inf_{p_n\in P_n(\mathcal{C})} \sup_{\mathbf{k}\in\mathcal{C}} |\omega(\mathbf{k}) - p_n(\mathbf{k})|.$$

However, the minimization of (4.2) is not trivial to solve for any type of domain in more than one dimension. Since the denominator of the Lagrange polynomials vanishes on a subset of $\mathcal{C}$,

the Lebesgue constant is not continuous with respect to the point set $\{\mathbf{k}_i\}_{i=1}^N$ in $\mathcal{C}^N$. Besides, $\Gamma_N(\{\mathbf{k}_i\}_{i=1}^N)$ is very sensitive to the location of the interpolation points, which makes the minimization procedure subtle. Although there have been several attempts to produce nodal sets using direct and indirect methods to minimize the Lebesgue constant, for example, Heinrichs directly minimized the Lebesgue constant in a triangular area with Fekete points as their initial guess [13], Babuška minimized norms of the Lagrange interpolation operator, which also yields small Lebesgue constant in a triangle [6], Sommariva provided the approximate Fekete and approximate optimal nodal points in the square and the triangle by solving numerically the corresponding optimization problems [4], nor are we able to find the exact optimal points. Thus, the question of how to sample points in $\mathcal{B}_{\text{red}}$ and $\tilde{\mathcal{B}}_{\text{red}}$ which are suitable for polynomial interpolation is still an open question.

Since in the multivariate case, the optimal Lagrange interpolant is hard to determine, our aim is to find a suitable sampling point set, on which our Lagrange interpolation performs well when dealing with the band function reconstruction.

4.1 Sampling points in triangle

To standardize the problem, let the right isosceles triangle T be the reference triangle,

$$T := \{\mathbf{x} = (x, y) : 0 \leqslant x \leqslant 1, 0 \leqslant y \leqslant 1 - x\},$$

and let $P_n(T)$ be the space of polynomials on T with degree at most n,

$$P_n(T) = \text{span}\{x^i y^j, \quad i + j \leqslant n\}.$$

In the following, we introduce several sampling methods on this reference triangle T.

Mean optimal points

The mean optimal nodal set is defined by minimizing a norm related to the Lagrange interpolation operator $\mathbf{L}$, which takes the form [6]

$$\|\mathbf{L}\|_2 := \int_T \sum_{i=1}^N |l_i(\mathbf{x})|^2 \mathrm{d}\mathbf{x}. \tag{4.3}$$

Here, $\{l_i(\mathbf{x})\}_{i=1}^N$ is defined in the same way as in (4.1). Compared with (4.2), the minimization of (4.3) involves less computational complexity and is thus more favorable. Indeed, suppose $\{p_i(\mathbf{x})\}_{i=1}^N$ is a set of standard orthogonal polynomials on the triangle T with degree at most n, i.e., $\int_T p_i(\mathbf{x}) p_j(\mathbf{x}) \mathrm{d}\mathbf{x} = \delta_{ij}$ for all $i, j = 1, \cdots, N$, then for any given point set $\{\mathbf{x}_j\}_{j=1}^N$, the Lagrange polynomials, if exist, can be expressed as $l_k(\mathbf{x}) = \sum_{i=1}^N a_{ki} p_i(\mathbf{x})$ with some constants $\{a_{ki}\}_{k,i=1}^N$, which allows (4.3) to be expressed as $\|\mathbf{L}\|_2 = \sum_{k=1}^N \sum_{i=1}^N |a_{ki}|^2$. In comparison, the calculation of $\Gamma_N(\{\mathbf{x}_i\}_{i=1}^N)$ is equivalent to the calculation of $\max_{\mathbf{x}\in T} \sum_{k=1}^N |\sum_{i=1}^N |a_{ki} p_i(\mathbf{x})|$, which has more computational complexity. Numerical results show that $\|\mathbf{L}\|_2 \backslash \Gamma_N \left(\{\mathbf{x}_i\}_{i=1}^N\right)$ is not large and the performance of this kind of point set is nearly optimal.

Fekete points

Fekete point set [2] is another kind of nearly optimal nodal point set that maximizes the absolute value of the determinant of Vandermonde matrix $V(\mathbf{x}_1, \mathbf{x}_2, \cdots, \mathbf{x}_N)$,

$$\max_{\{\mathbf{x}_1, \mathbf{x}_2, \cdots, \mathbf{x}_N\} \subset T} \left| \det(V(\mathbf{x}_1, \mathbf{x}_2, \cdots, \mathbf{x}_N)) \right|. \tag{4.4}$$

Here, $V(\mathbf{x}_1, \mathbf{x}_2, \cdots, \mathbf{x}_N)$ is of size $N \times N$ with entries

$$V_{ij} = g_j(\mathbf{x}_i) \text{ for } i, j = 1, \cdots, N.$$

$\{g_i\}_{i=1}^N$ denotes a set of basis functions in $P_n(T)$. Note that $\det(V)$ can be regarded as a polynomial function of $(\mathbf{x}_1, \cdots, \mathbf{x}_n)$, which implies the existence of Fekete points for a given compact set T. Note also that Problem (4.4) involves less computational complexity than the minimization of (4.2). As the first attempt, Bos [2] constructed the Fekete point set up to the 7th order, which was further extended up to degree 13 [6] and 18 [32] in a triangle, respectively.

Improved Lobatto grid

The improved Lobatto grid is proposed in [1] as an improvement of the original Lobatto grid, which composes of (ξ_i, η_j) defined by

$$\xi_i = \frac{1}{3}(1 + 2v_j - v_i - v_k), \eta_j = \frac{1}{3}(1 + 2v_i - v_j - v_k) \text{ for } i = 1, \cdots, n+1 \text{ and } j = 1, \cdots, n+2-i.$$

Here, $k := n + 3 - i - j$ and $v_i := \frac{1}{2}(1 + t_i)$ with t_i denoting the zeros of the nth degree Labatto polynomials.

This proposed point set utilizes the zeros of Lobatto polynomials which are close to optimal for 1D interpolation [8]. It is generated by deploying Lobatto interpolation nodes along the three edges of the triangle, and then computing interior nodes by averaged intersections to achieve three-fold rotational symmetry. The symmetry of the distribution with respect to the three vertices is a significant improvement of the original Lobatto grid. Its straightforward implementation makes it an attractive choice, and numerical results show that the Lebesgue constant for this point set is competitive with the above mentioned two point sets.

The following figures show the comparison of mean optimal points, Fekete points, and the improved Lobatto grid for $n = 4, 8$.

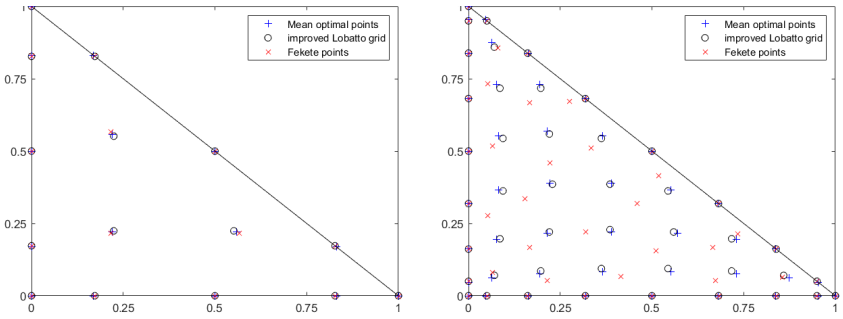

(a) $n = 4$ (b) $n = 8$

Figure 2: Mean optimal points, Fekete points, and improved Lobatto grid for $n = 4, 8$.

Remark 4.1 (Lebesgue constants for mean optimal points, Fekete points and improved Lobatto grid)**.** *Although there is no rigorous proof on the boundedness of the Lebesgue constants for mean optimal points, Fekete points and improved Lobatto grid, numerical evidence [6, 32, 1] suggests that their Lebesgue constants are proportional to* $\sqrt{N}$.

4.2 Sampling points in quadrilateral

For a quadrilateral, we will first project it into the unit square $S := [-1, 1]^2$ by projective mapping [12] and then consider the polynomial space with two variables and degree at most n in each variable, i.e.,

$$P_n(S) = \text{span}\{x^i y^j, \quad i, j \leqslant n\}.$$

It is well known that in 1D case, interpolation using the zeros of Chebyshev polynomials is close to optimal. So in the case of unit square, we mainly consider the following two sampling point sets with tensor product:

The Chebyshev points of the first kind (Cheb1) in the interval $[-1, 1]$ are the zeros of the Chebyshev polynomial of the first kind $T_{n+1}(x)$,

$$x_k = \cos \frac{2k+1}{2(n+1)}\pi, \quad k = 0, \cdots, n.$$

The Chebyshev points of the second kind (Cheb2) in the interval $[-1, 1]$ are the zeros of the Chebyshev polynomial of the second kind $U_{n-1}(x)$ times $(x^2 - 1)$, i.e.,

$$x_i = \cos\left(\frac{i}{n}\pi\right), \quad i = 0, \cdots, n.$$

Figure 3 demonstrates the comparison of Cheb1 and Cheb2 for $n = 4$ and $n = 8$ after using tensor product to expand them to the unit square.

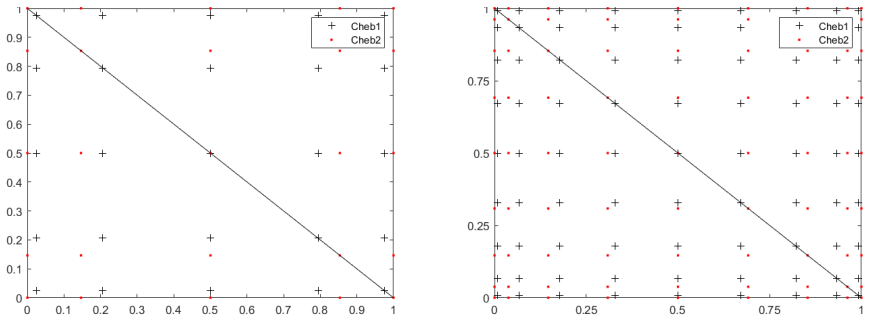

(a) $n = 4$ (b) $n = 8$

Figure 3: Cheb1 and Cheb2 with tensor product for $n = 4, 8$.

Remark 4.2 (Lebesgue constants for Cheb1 and Cheb2)**.** *Since the Lebesgue constants of* Cheb1 *and* Cheb2 *are both proportional to* $\log(N)$ *[15], where* $N = n + 1$ *is the dimension of the polynomial space in* $[-1, 1]$*, the Lebesgue constants of our nodal point sets are proportional to* $(\log(N))^2$*, where* $N = (n + 1)^2$ *is the dimension of the polynomial space with two variables and degree at most* n *in each variable.*

Remark 4.3 (Comparison of computational complexity)**.** *It is worth noticing that the computational complexity for* (4.1) *is consistent corresponding to all these five sampling methods, even though the number of Chebyshev points is almost twice as the number of those three kinds of sampling points within the triangular area, due to the mirror and rotational symmetry mentioned earlier. For example, in Figure 3(a), we have 25 Chebyshev points, but we only need to compute eigenvalues at 15 of them within the right isosceles triangle.*

Remark 4.4. *Considering the importance of the edges of the IBZ* $\partial\mathcal{B}_{\text{red}}$*, we expect that the performance of* Cheb2 *is better than that of* Cheb1*. The numerical results presented in the next section can further confirm this speculation.*

5 Numerical experiments

To demonstrate the performance of our proposed method (4.1) together with the sampling methods presented in Sections 4.1 and 4.2, we mainly consider PhCs with a square unit cell as in Figure 4 and a hexagonal unit cell as in Figure 5. We calculate the eigenvalue problem for a given sampling point using the conforming Galerkin Finite Element method.

Figure 4: Square lattice: unit cell (left) and the corresponding first Brillouin zone (right). The IBZ is the blue area with vertices $\Gamma = (0,0)$, $X = \frac{1}{a}(\pi, 0)$ and $M = \frac{1}{a}(\pi, \pi)$.

Figure 5: Hexagonal lattice: unit cell (left) and the corresponding first Brillouin zone (right). The IBZ is the blue area with vertices $\Gamma = (0,0)$, $K = \frac{1}{a}(\frac{4}{3}\pi, 0)$ and $M = \frac{1}{a}(\pi, \frac{\sqrt{3}}{3}\pi)$.

Due to the high contrast between the relative permittivity of the circular medium and its external medium, we utilize a fitted mesh $\mathcal{T}_h$ generated by *distmesh2d* provided by Persson and Strang to avoid the stabilization issue when an unfitted mesh is used, which is depicted in Figures 6(a) and 6(b). Here, we choose mesh size $h = 0.025a$ for square lattice and $h = 0.05a$ for hexagonal lattice. The associated conforming piecewise affine space is

$$V_h = \{v_h \in C(\overline{\Omega}) : v_h|_K \in P_1(K) \ \text{ for all } K \in \mathcal{T}_h\}.$$

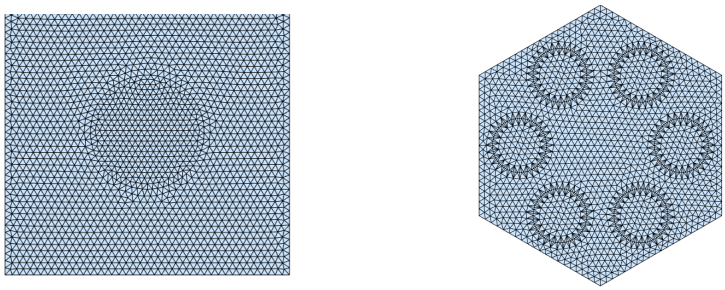

(a) Square lattice #DOFs=2107 (b) Hexagonal lattice #DOFs=1781

Figure 6: Discretization of the unit cell Ω by *distmesh2d*.

Given $\mathbf{k} \in \mathcal{B}$, the conforming Galerkin Finite Element approximation to Problem (3.4) reads as finding non-trivial eigenpair $(\lambda_h, u_h) \in (\mathbb{R}, V_h)$, satisfying

$$\begin{cases} a(u_h, v_h) = \lambda b(u_h, v_h) \text{ for all } v \in V_h \\ b(u_h, u_h) = 1. \end{cases} \tag{5.1}$$

Note that $\mathcal{B}_{\text{red}}$ is a triangle for both cases. We map it into the right isosceles triangle and use $\hat{\mathcal{B}}$ which is composed of 253 evenly distributed points shown in Figure 7(a) and Figure 7(b) as the reference solution. The pointwise relative error is defined as

$$e_i(\mathbf{k}) := \frac{|\omega_i(\mathbf{k}) - \mathbf{L}\omega_i(\mathbf{k})|}{\omega_i(\mathbf{k})} \quad \text{for } \mathbf{k} \in \hat{\mathcal{B}} \text{ and } i = 1, \cdots, 6.$$

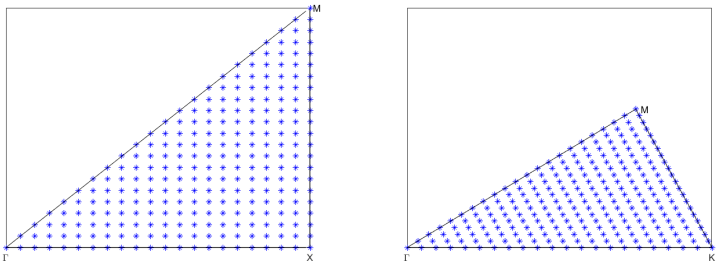

(a) 253 evenly distributed points in the IBZ of square lattice. (b) 253 evenly distributed points in the IBZ of hexagonal lattice.

Figure 7: $\hat{\mathcal{B}}$.

Here, $\omega_i(\mathbf{k})$ is ith band function obtained directly by the conforming Galerkin Finite Element method over $\hat{\mathcal{B}}$ using the same mesh on the unit cell Ω, and $\mathbf{L}\omega_i(\mathbf{k})$ is the Lagrange interpolation (4.1) with a certain sampling method. In specific, we use maximum relative error and average relative error to investigate the performance of our methods, which are defined by

$$\text{error}_\infty := \max_{i=1,\cdots,6} \max_{\mathbf{k}\in\hat{\mathcal{B}}} |e_i(\mathbf{k})| \text{ and } \text{error}_{\text{avg}} := \frac{1}{253} \sum_{\mathbf{k}\in\hat{\mathcal{B}}} \left(\frac{1}{6} \sum_{i=1}^{6} |e_i(\mathbf{k})| \right).$$

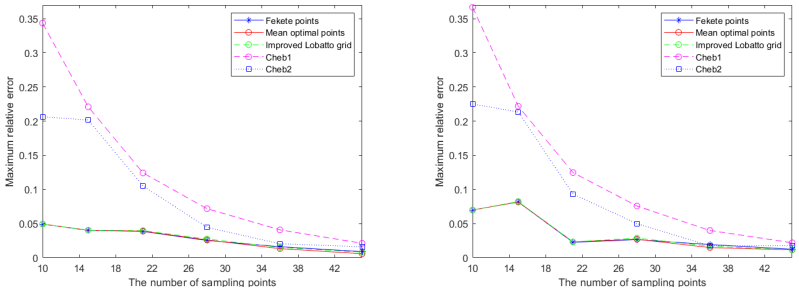

(a) TM mode (b) TE mode

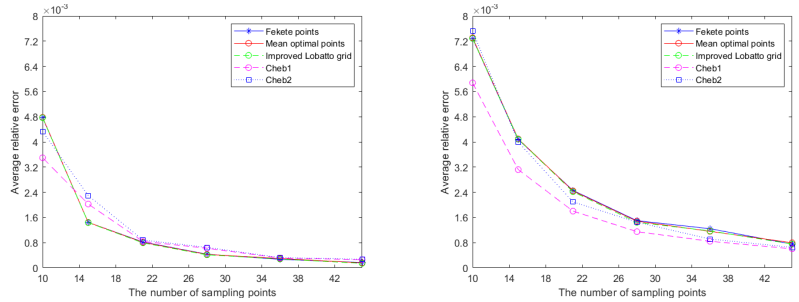

(c) TM mode (d) TE mode

Figure 8: Square lattice: the performance of (4.1) under error_∞ and $\text{error}_{\text{avg}}$.

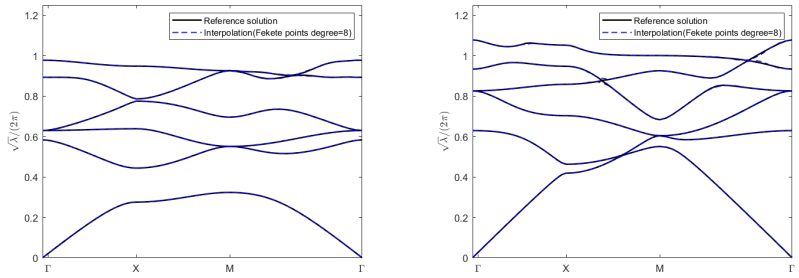

(a) TM mode (b) TE mode

(c) TM mode (d) TE mode

Figure 9: Square lattice: band functions along $\partial\mathcal{B}_{\text{red}}$ using Fekete points and Cheb2 with degree $n = 8$.

5.1 Numerical tests with square lattice in Figure 4

In this section, we are concerned with the case of square lattice as in Figure 4, wherein the lattice vectors are $\mathbf{a}_1 = a(0,1)^T$, and $\mathbf{a}_2 = a(1,0)^T$ with a positive parameter a. The circle area has radius $r = 0.2a$ and $\epsilon = 8.9$ (as for alumina) which is embedded in air ($\epsilon = 1$). In this case, due to the symmetry of the first Brillouin zone $\mathcal{B}$, we can restrict the sampling points $\mathbf{k}$ to the triangle $\mathcal{B}_{\text{red}}$ and apply the sampling methods in Subsection 4.1. Alternatively, we can sample $\mathbf{k}$ in a quadrilateral $\tilde{\mathcal{B}}_{\text{red}}$ composed of $\mathcal{B}_{\text{red}}$ and the its symmetric area along its longest edge, then consider the sampling methods in Subsection 4.2.

The performance of Lagrange interpolation on those five kinds of sampling points is shown in Figure 8. Note that the horizontal axis shows the number of sampling points inside $\mathcal{B}_{\text{red}}$. Figure 9 depicts the approximate band structure along the edges of the irreducible Brillouin zone using Fekete points and Cheb2 with degree $n = 8$.

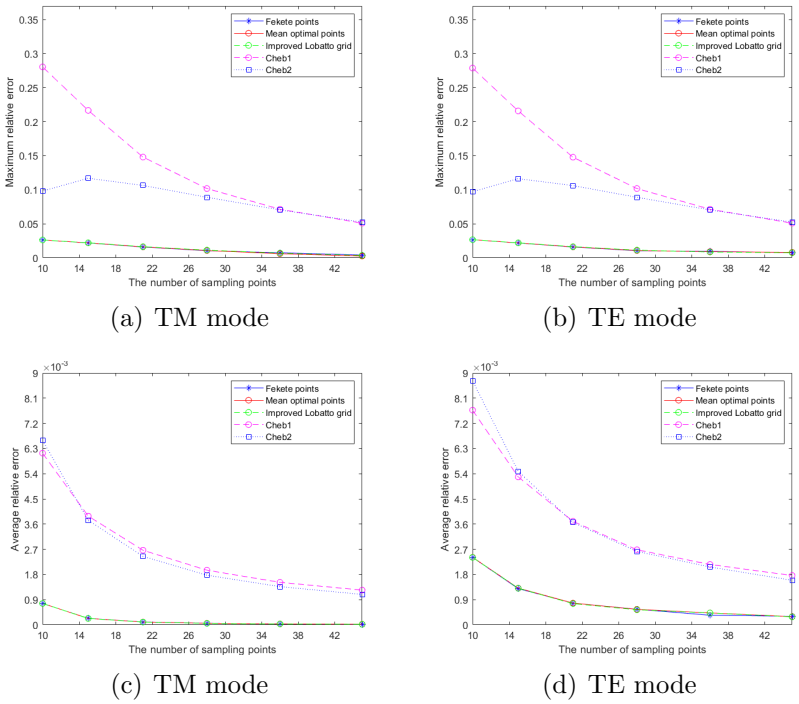

(a) TM mode (b) TE mode

(c) TM mode (d) TE mode

Figure 10: Hexagonal lattice: the performance of (4.1) under error_∞ and $\text{error}_{\text{avg}}$.

5.2 Numerical tests with hexagonal lattice in Figure 5

In this section, we focus on another kind of 2D PhCs which has infinite periodic hexagonal lattice. As shown in Figure 5, its unit cell is composed of six cylinders of dielectric material with dielectric constant $\epsilon = 8.9$ embedded in the air. The lattice vectors are $\mathbf{a}_1 := a(1,0)^T$ and $\mathbf{a}_2 := a(\frac{1}{2}, \frac{\sqrt{3}}{2})^T$ with lattice constant $a = 3R$. The radius of cylinders is $r = \frac{1}{3}R$. Here, the positive parameter R denotes the length of hexagon edges. In this case, due to the symmetry of the first Brillouin zone, we can restrict the wave vector $\mathbf{k}$ to $\mathcal{B}_{\text{red}}$ or $\tilde{\mathcal{B}}_{\text{red}}$ which is composed of $\mathcal{B}_{\text{red}}$ and the symmetric area of $\mathcal{B}_{\text{red}}$ along its longest edge.

In Figure 10, we display the performance of Lagrange interpolation methods (4.1) based upon those five types of sampling methods measured in error_∞ and $\text{error}_{\text{avg}}$ against the number of sampling points inside $\mathcal{B}_{\text{red}}$. One can observe excellent performance for all cases from Figures

8 and 10. For instance, 45 sampling points inside $\mathcal{B}_{\text{red}}$ leads to error$_\infty$ below 1% depending on the choice of sampling methods as well as the smoothness of the band functions. Note that the performance for hexagonal unit cell is typically better than that for the square unit cell since the first six band functions are smoother in the former case. One can infer the regularity of band functions along the edges of $\mathcal{B}_{\text{red}}$. We observe from Figures 11 and 9 that the band functions with square lattice exhibit a larger and more diverse frequency distribution range, resulting in more singularities. Besides, we can also observe from Figures 8 and 10 that the performance of Lagrange interpolation based upon the first three sampling methods (Fekete points, mean optimal points and improved Lobatto grid) in both TE mode and TM mode, are similar or better than Cheb1 and Cheb2.

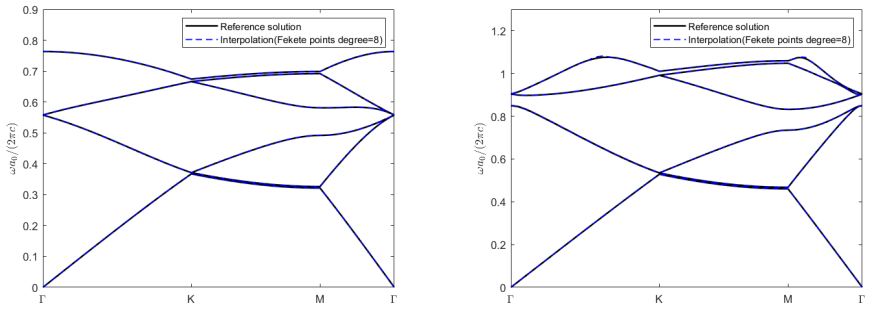

(a) TM mode

(b) TE mode

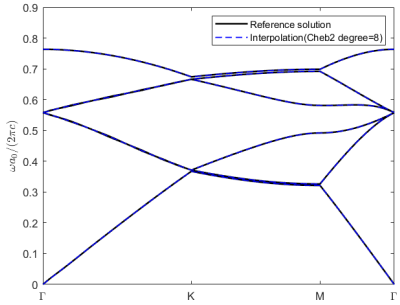

(c) TM mode

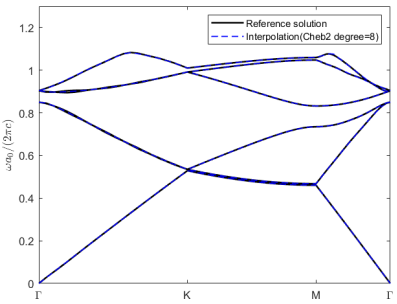

(d) TE mode

Figure 11: Hexagonal lattice: band functions along the edges of the irreducible Brillouin zone using Fekete points and Cheb2 with degree $n = 8$.

Figure 11 illustrates the approximate band structure along the edges of the irreducible Brillouin zone using Fekete points and Cheb2 with degree $n = 8$, showing that the approximate band functions match the ground truth well within a reasonable accuracy. Together with Figure 9, we conclude that all those five methods can provide reasonably good reconstruction. Figure 12 shows a zoomed-in view of some special points in Figures 9 and 11. We can observe that the areas with large interpolation errors are clearly the areas where the adjacent band functions are very close, which is consistent with the conclusion we have drawn before that the branch points are singular points.

Note that it is quite difficult or even impossible to identify all branch points or distinguish from a fake branch point where two adjacent band functions are close but without intersecting due to many factors, for example the rounding error and numerical error resulting from (5.1). As a result, our numerical method can only yield approximative branch points where the adjacent

band functions are close. Nevertheless, the overall performance demonstrates that our method is capable of approximating the band functions of 2-dimension PhCs within a reasonable accuracy.

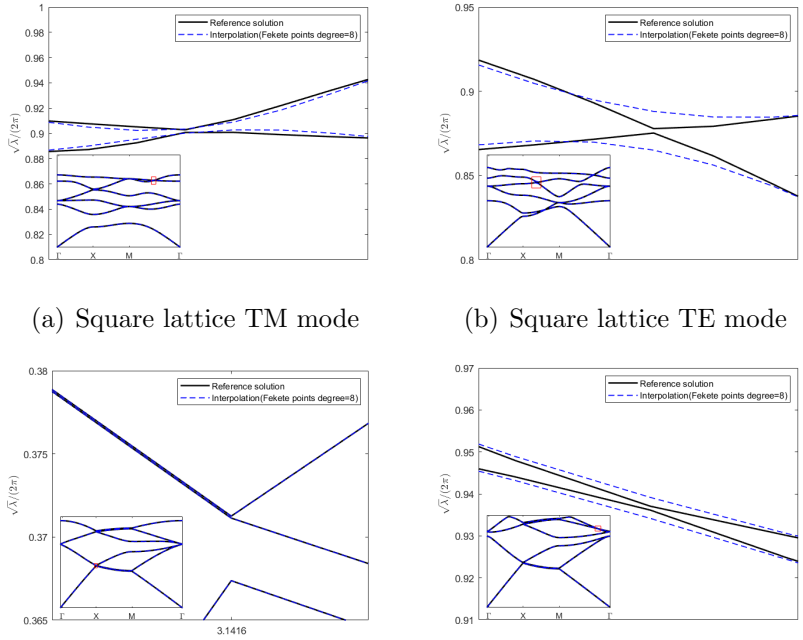

(a) Square lattice TM mode (b) Square lattice TE mode

(c) Hexagonal lattice TM mode (d) Hexagonal lattice TE mode

Figure 12: Zoom-in to the interpolation results within the red box area.

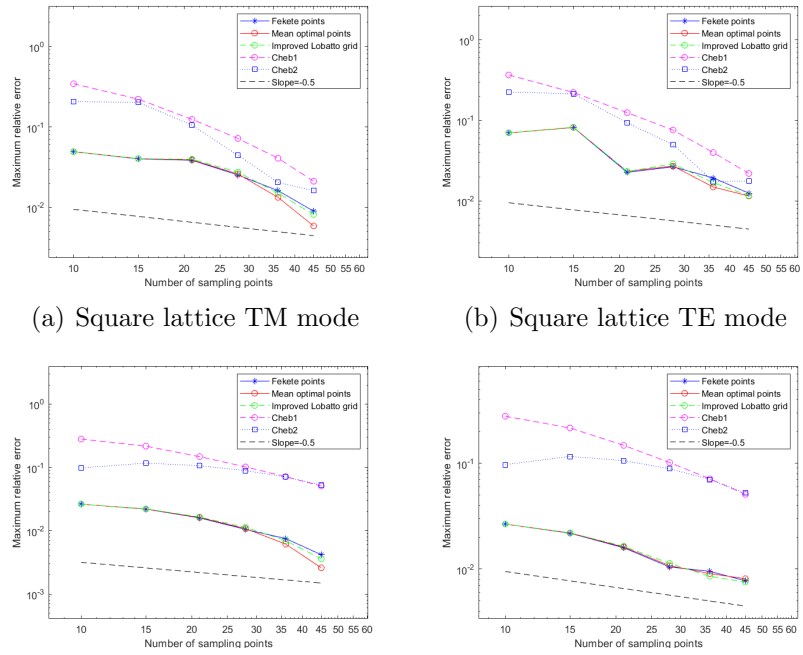

(a) Square lattice TM mode (b) Square lattice TE mode

(c) Hexagonal lattice TM mode (d) Hexagonal lattice TE mode

Figure 13: Convergence results.

We present in Figure 13 the convergence of our proposed method for the crystals with both

square lattice and hexagonal lattice for the TM mode and TE mode. We observe algebraic convergence and the slopes of these five sampling methods are similar as we expected from the approximation theory [33].

6 Conclusion

In this paper, we analyze the properties of photonic band functions and consider the problem of band structure reconstruction in the context of two-dimensional periodic PhCs. The regularity of band functions is crucial for our proposed approximation method. In contrast to the traditional sampling algorithms based upon global polynomial interpolation and limited to the edges of the irreducible Brillouin zone, we propose an efficient and accurate global approximation algorithm based upon the Lagrange interpolation methods for computing band functions over the whole first Brillouin zone. Regarding the selection of sampling points, we consider five different sampling algorithms to select suitable interpolation points in the first Brillouin zone or the irreducible Brillouin zone. We observe algebraic convergence rate and the numerical tests demonstrate that our method can approximate band functions efficiently. For example, our methods reach relative error below 1% using only 45 sampling points. It should be noted that we focus on sampling algorithms based upon global polynomial interpolation in this paper since this is the current Start-Of-The-Art. However, this current method cannot identify branch points quite efficiently, since the global interpolation approximation has a relatively slow convergence rate due to the piecewise analyticity of the band functions. In order to make better use of this property, we will explore adaptive sampling algorithms based upon piecewise polynomial interpolation in the future for better performance.

Acknowledgments

Y. W. acknowledges support from the Research Grants Council (RGC) of Hong Kong via the Hong Kong PhD Fellowship Scheme (HKPFS). G.L. acknowledges support from Newton International Fellowships Alumni following-on funding awarded by The Royal Society and Early Career Scheme (Project number: 27301921), RGC, Hong Kong. We thank Richard Craster (Imperial College London) for fruitful discussion.

References

[1] M. Blyth and C. Pozrikidis. A lobatto interpolation grid over the triangle. *IMA journal of applied mathematics*, 71(1):153–169, 2006.

[2] L. Bos. On certain configurations of points in rn which are unisolvent for polynomial interpolation. *Journal of approximation theory*, 64(3):271–280, 1991.

[3] L. Bos, S. De Marchi, A. Sommariva, and M. Vianello. Computing multivariate fekete and leja points by numerical linear algebra. *SIAM Journal on Numerical Analysis*, 48(5):1984–1999, 2010.

[4] M. Briani, A. Sommariva, and M. Vianello. Computing fekete and lebesgue points: simplex, square, disk. *Journal of Computational and Applied Mathematics*, 236(9):2477–2486, 2012.

[5] C. Canuto, M. Hussaini, A. Quarteroni, and T. Zang. *Spectral methods: fundamentals in single domains*. Springer Science & Business Media, 2007.

[6] Q. Chen and I. Babuška. Approximate optimal points for polynomial interpolation of real functions in an interval and in a triangle. *Computer Methods in Applied Mechanics and Engineering*, 128(3-4):405–417, 1995.

[7] R. Craster, T. Antonakakis, M. Makwana, and S. Guenneau. Dangers of using the edges of the brillouin zone. *Physical Review B*, 86(11):115130, 2012.

[8] L. Fejér. Lagrangesche interpolation und die zugehörigen konjugierten punkte. *Mathematische Annalen*, 106(1):1–55, 1932.

[9] S. Giani and I. Graham. Adaptive finite element methods for computing band gaps in photonic crystals. *Numerische Mathematik*, 121(1):31–64, 2012.

[10] I. Glazman. *Direct methods of qualitative spectral analysis of singular differential operators*, volume 2146. Israel Program for Scientific Translations, 1965.

[11] J. Harrison, P. Kuchment, A. Sobolev, and B. Winn. On occurrence of spectral edges for periodic operators inside the brillouin zone. *Journal of Physics A: Mathematical and Theoretical*, 40(27):7597, 2007.

[12] P. Heckbert. Projective mappings for image warping. *Image-Based Modeling and Rendering*, 869, 1999.

[13] W. Heinrichs. Improved lebesgue constants on the triangle. *Journal of Computational Physics*, 207(2):625–638, 2005.

[14] M. Hussein. Reduced bloch mode expansion for periodic media band structure calculations. *Proceedings of the Royal Society A: Mathematical, Physical and Engineering Sciences*, 465(2109):2825–2848, 2009.

[15] B. Ibrahimoglu. Lebesgue functions and lebesgue constants in polynomial interpolation. *Journal of Inequalities and Applications*, 2016(1):1–15, 2016.

[16] J. Jackson. Classical electrodynamics, 1999.

[17] J. Joannopoulos, S. Johnson, J. Winn, and R. Meade. Molding the flow of light. *Princeton Univ. Press, Princeton, NJ [ua]*, 2008.

[18] P. Jorkowski and R. Schuhmann. Higher-order sensitivity analysis of periodic 3-d eigenvalue problems for electromagnetic field calculations. *Advances in Radio Science*, 15:215–221, 2017.

[19] P. Jorkowski and R. Schuhmann. Mode tracking for parametrized eigenvalue problems in computational electromagnetics. In *2018 International Applied Computational Electromagnetics Society Symposium (ACES)*, pages 1–2. IEEE, 2018.

[20] T. Kato. *Perturbation theory for linear operators*, volume 132. Springer Science & Business Media, 2013.

[21] L. Kaup and B. Kaup. *Holomorphic functions of several variables: an introduction to the fundamental theory*, volume 3. Walter de Gruyter, 2011.

[22] C. Kittel and P. McEuen. *Introduction to solid state physics*. John Wiley & Sons, 2018.

[23] D. Klindworth and K. Schmidt. An efficient calculation of photonic crystal band structures using taylor expansions. *Communications in Computational Physics*, 16(5):1355–1388, 2014.

[24] P. Kuchment. *Floquet theory for partial differential equations*, volume 60. Springer Science & Business Media, 1993.

[25] D. Labilloy, H. Benisty, C. Weisbuch, T. Krauss, V. Bardinal, and U. Oesterle. Demonstration of cavity mode between two-dimensional photonic-crystal mirrors. *Electronics Letters*, 33(23):1978–1980, 1997.

[26] F. Maurin, C. Claeys, E. Deckers, and W. Desmet. Probability that a band-gap extremum is located on the irreducible brillouin-zone contour for the 17 different plane crystallographic lattices. *International Journal of Solids and Structures*, 135:26–36, 2018.

[27] P. Russell. Photonic crystal fibers. *science*, 299(5605):358–362, 2003.

[28] H. Salzer. Lagrangian interpolation at the chebyshev points xn, $\nu \equiv \cos(\nu\pi/\mathrm{n})$, $\nu = 0\ (1)\ \mathrm{n}$; some unnoted advantages. *The Computer Journal*, 15(2):156–159, 1972.

[29] S. Sauter and C. Schwab. Boundary element methods. In *Boundary Element Methods*, pages 183–287. Springer, 2010.

[30] C. Scheiber, A. Schultschik, O. Biro, and R. Dyczij-Edlinger. A model order reduction method for efficient band structure calculations of photonic crystals. *IEEE transactions on magnetics*, 47(5):1534–1537, 2011.

[31] K. Schmidt and P. Kauf. Computation of the band structure of two-dimensional photonic crystals with hp finite elements. *Computer Methods in Applied Mechanics and Engineering*, 198(13-14):1249–1259, 2009.

[32] M. Taylor, B. Wingate, and R. Vincent. An algorithm for computing fekete points in the triangle. *SIAM Journal on Numerical Analysis*, 38(5):1707–1720, 2000.

[33] A. Timan. *Theory of approximation of functions of a real variable*. Elsevier, 2014.

[34] L. Trefethen. *Approximation Theory and Approximation Practice, Extended Edition*. SIAM, 2019.

[35] S. Wang. *Numerical study of thermal-hydraulic-mechanical behavior of fractured geothermal reservoirs*. Colorado School of Mines, 2015.

[36] C. Wilcox. Theory of bloch waves. *Journal d'Analyse Mathématique*, 33(1):146–167, 1978.

[37] M. Yanik, S. Fan, M. Soljačić, and J. Joannopoulos. All-optical transistor action with bistable switching in a photonic crystal cross-waveguide geometry. *Optics letters*, 28(24):2506–2508, 2003.